ACS OMEGA

Open Access

http://pubs.acs.org/journal/acsodf

Article

Characterization of LL37 Binding to Collagen through Peptide Modification with a Collagen-Binding Domain

Ziqi Wei, Marsha W. Rolle, and Terri A. Camesano*

Cite This: *ACS Omega* 2023, 8, 35370−35381

Read Online

ACCESS | Metrics & More | Article Recommendations | Supporting Information

ABSTRACT: Collagen-based biomaterials loaded with antimicrobial peptides (AMPs) present a promising approach for promoting wound healing while providing protection against infections. In our previous work, we modified the AMP LL37 by incorporating a collagen-binding domain (cCBD) as an anchoring unit for collagen-based wound dressings. We demonstrated that cCBD-modified LL37 (cCBD-LL37) exhibited improved retention on collagen after washing with PBS. However, the binding mechanism of cCBD-LL37 to collagen remained to be elucidated. In this study, we found that cCBD-LL37 showed a slightly higher affinity for collagen compared to LL37. Our results indicated that cCBD inhibited cCBD-LL37 binding to collagen but did not fully eliminate the binding. This suggests that cCBD-LL37 binding to collagen may involve more than just one-site-specific binding through the collagen-binding domain, with non-specific interactions also playing a role. Electrostatic studies revealed that both LL37 and cCBD-LL37 interact with collagen via long-range electrostatic forces, initiating low-affinity binding that transitions to close-range or hydrophobic interactions. Circular dichroism analysis showed that cCBD-LL37 exhibited enhanced structural stability compared to LL37 under varying ionic strengths and pH conditions, implying potential improvements in antimicrobial activity. Moreover, we demonstrated that the release of LL37 and cCBD-LL37 into the surrounding medium was influenced by the electrostatic environment, but cCBD could enhance the retention of peptide on collagen scaffolds. Collectively, these results provide important insights into cCBD-modified AMP-binding mechanisms and suggest that the addition of cCBD may enhance peptide structural stability and retention under varying electrostatic conditions.

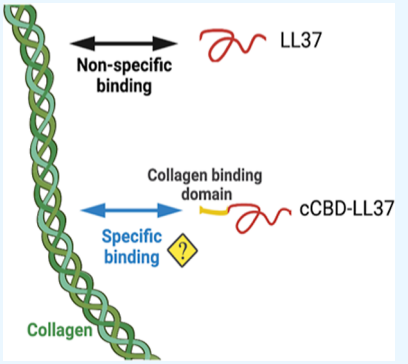

1. INTRODUCTION

Wound healing, a complex biological process, is vital for restoring tissue function post-injury or surgery.[1] Factors like age, comorbidities, and wound severity can obstruct this process, causing chronic or non-healing wounds.[2] This imposes a heavy burden on healthcare systems and patients, highlighting the need for advanced therapeutic strategies.[3] Biomaterials, both synthetic and natural, are emerging as a potential solution to wound healing complications by adjusting the healing milieu and promoting tissue restoration.[4] These materials can be engineered into different forms like hydrogels, films, or scaffolds, mimicking the extracellular matrix and facilitating the delivery of bioactive agents. Collagen is essential for maintaining the integrity and functionality of various human tissues.[5,6] Its unique properties make it a popular biomaterial for numerous biomedical applications, such as tissue engineering, drug delivery, and wound healing.

LL37, a 37-amino acid cationic peptide from the cathelicidin family, exhibits broad-spectrum antimicrobial activity.[7−9] LL37 exerts its antimicrobial activity primarily by disrupting microbial membranes, leading to cell lysis.[10] Importantly, beyond its antimicrobial activity, LL37 influences several aspects of wound repair and regeneration. It has been shown to modulate immune responses,[11] reducing inflammation[12] while also recruiting and activating cells for wound healing.[13] Furthermore, it promotes reepithelization and angiogenesis, essential steps for wound closure and restoration of tissue function.[14] To effectively harness these properties for wound healing, the immobilization of LL37 onto collagen through a collagen-binding domain (cCBD) has been proposed.[15−17]

A cCBD with selective affinity for collagen, TKKTLRT (collagenase CBD; cCBD), has been identified.[15,18,19] Our lab developed a chimeric peptide, cCBD-LL37, by adding the collagen-binding domain TKKTLRT to the C-terminus of LL37, enabling the peptide to specifically bind to the collagen scaffold. We then quantified the binding of LL37 and cCBD-LL37 to collagen using a quartz crystal microbalance with dissipation monitoring (QCM-D). The results showed no significant difference between the binding of LL37 and cCBD-LL37 to collagen; however, cCBD-LL37 exhibited enhanced retention on collagen after washing with PBS.[20] Although the prior study provided an effective strategy for quantifying both

Received: July 23, 2023
Accepted: August 31, 2023
Published: September 14, 2023

unmodified and cCBD-modified peptides binding to collagen, it did not characterize the peptide-collagen binding mechanism, such as whether it involved electrostatic interactions or binding via the cCBD.

Understanding the factors that influence LL37 and cCBD-LL37 binding to collagen is crucial for optimizing the dosing of antimicrobial peptide (AMP) or cCBD-AMP-loaded collagen wound dressings and designing cCBD-AMP delivery systems. The factors that influence proteins−collagen interactions differ significantly. Romijn et al. reported that von Willebrand factor binds to collagen triple helix through hydrophobic interactions and positively charged domains.[21] Sasaki et al. suggested osteonectin binds to collagen due to a combination of van der Waals and electrostatic interactions.[22] LL37 has a charge of +6 at physiological pH, and cCBD-LL37 retains the same +6 charge with the addition of cCBD, indicating that electrostatic interactions could be involved in the binding of cCBD-LL37 to collagen.

In this study, our aim was to characterize the cCBD strategy for delivering AMPs via collagen-based scaffolds. We hypothesized that the positively charged LL37 may bind nonspecifically to the negatively charged groups on the collagen surface. As cCBD-LL37 retains the same positive charge with LL37, nonspecific interactions are likely one of the components during binding, but the cCBD may also aid in the formation of high-affinity binding. We investigated the role of the electrostatic interactions in LL37 and cCBD-LL37 binding to collagen, compared the conformational stability of LL37 and cCBD-LL37 under changing electrostatic environments, and explored the retention of AMPs on collagen scaffolds under varying electrostatic conditions.

2. MATERIALS AND METHODS

2.1. Peptides and Reagents. Nutragen Type I collagen from bovine hides (Advanced BioMatrix, Carlsbad, CA) was received in solution (5.9 mg/mL). To obtain the desired concentrations of 0.1 mg/mL, the collagen solution was diluted in phosphate-buffered saline (PBS, pH ∼7.4) at 4 °C (Sigma-Aldrich, St. Louis, MO). LL37 (LLGDFFRKSKEKIGKEFKRIVQRIKDFLRNLVPRTES) was purchased from Anaspec (Fremont, CA) in lyophilized form, synthesized at ≥95% purity. cCBD-LL37 (LLGDFFRKSKEKIGKEFKRIVQRIKDFLRNLVPRTESDYKDDDDKTKKTLRT) was purchased from New England Peptide (Gardner, MA) in lyophilized form, synthesized at ≥90% purity. cCBD (DYKDDDDKTKKTLRT) was purchased from Bachem (Torrance, CA) in lyophilized form, synthesized at ≥95% purity. Both cCBD-LL37 and cCBD were designed to include a FLAG linker (DYKDDDDK) as an epitope tag.

2.2. Detection of AMPs Binding to Collagen. The binding of LL37 and cCBD-LL37 to type I collagen was studied by a modification of the method of Calderwood et al.[23] Type I collagen in PBS was incubated overnight at 4 °C in 96-well Brand microplates. Wells were blocked with 1% w/v bovine serum albumin (BSA) in PBS for 1 h at room temperature and then incubated with LL37 or cCBD-LL37 for 1 h at room temperature. The wells were incubated overnight at 4 °C with polyclonal rabbit anti-human LL37 antibody (0.4 μg/mL, AnaSpec, #AS-55927) and subsequently incubated at room temperature for 1 h with horseradish peroxidase-conjugated goat anti-rabbit antibody (0.3 μg/mLBio-Rad, #1706515). The bound proteins were then detected using 1-Step TMB (Thermo Scientific, #34024). The reaction was stopped after 10 min by the addition of 2.5 M H_2SO_4, and the absorbance was read at 450 nm. The data were fitted to a one-site binding model using GraphPad Prism.

2.3. Inhibition of AMPs Binding by cCBD. The inhibition of AMP binding by cCBD was studied by a modification of the method of Ishihara et al.[24] Brand microplates were coated with type I collagen overnight at 4 °C. Then, the wells were blocked with 1% w/v BSA and further incubated with 500 nM cCBD-LL37 for 1 h at room temperature with 0−500 nM cCBD. Next, the wells were incubated with polyclonal rabbit anti-human LL37 antibody (0.4 μg/mL, AnaSpec, #AS-55927). The antibody was detected by horseradish peroxidase-conjugated goat anti-rabbit antibody (0.3 μg/mL, Bio-Rad, #1706515). Color development and absorbance measurement were done as described above.

2.4. Characterization of the Interaction between Type I Collagen and AMPs. The assay to measure the binding of AMPs to collagen was modified to allow for the examination of the role of electrostatic interactions in the binding of LL37 and cCBD-LL37 to collagen. Brand microplates were coated with type I collagen overnight at 4 °C. Wells were blocked with 1% w/v BSA. LL37 or cCBD-LL37 was added at a concentration of 0.5 μM for 1 h at room temperature. After washing away unbound peptide with PBS, pH 7.4, wells were incubated with PBS buffers at the indicated pH levels for 10 min and washed three times at the indicated pH. Next, the wells were incubated with polyclonal rabbit anti-human LL37 antibody (0.4 μg/mL, AnaSpec, #AS-55927). The antibody was detected by horseradish peroxidase-conjugated goat anti-rabbit antibody (0.3 μg/mL, Bio-Rad, #1706515). Color development and absorbance measurement were done as described above. Similarly, ionic strength dependency was investigated by utilizing PBS, pH 7.4, containing a range of NaCl concentrations, from 0 to 500 mM. The effect of divalent cations on collagen binding was examined using increasing concentrations of $MgCl_2$ or $CaCl_2$ in PBS, pH 7.4, during protein binding and in all washes. The LL37 and cCBD-LL37 binding to collagen under varying ionic strength and pH as percentage of the initial protein loaded was plotted.

2.5. Circular Dichroism Spectroscopy. The influence of pH and ionic strength on the conformation of LL37 and cCBD-LL37 was studied by circular dichroism (CD) spectroscopy. The CD spectra of both peptides were acquired in quartz cells with a 0.1 cm path length (Jasco, #0556) at 23 °C using Jasco J-1500 CD spectrometer. The AMPs were studied at 10 μM in 5 mM sodium phosphate buffer, with adjusting NaCl, $MgCl_2$, or $CaCl_2$. Spectra corresponding to varying ionic strengths were documented within the 200−250 nm wavelength range, as wavelengths below 200 nm exhibited high absorbance due to increased salt concentrations. Similarly, the AMPs were studied at 10 μM in pH adjusted 5 mM sodium phosphate buffer. It has been observed that the helical structure of LL37 becomes entirely disordered in acidic conditions yet retains its structure in an alkaline environment.[25] Therefore, the CD spectra of both LL37 and cCBD-LL37 were evaluated across a pH range of 2−10. The spectra under varying pH were recorded between 190 and 250 nm. A baseline with buffer only was recorded separately and subtracted from each spectrum. The content of specific secondary structures (helix, strand, turn, and unordered) was

https://doi.org/10.1021/acsomega.3c05328
ACS Omega 2023, 8, 35370−35381

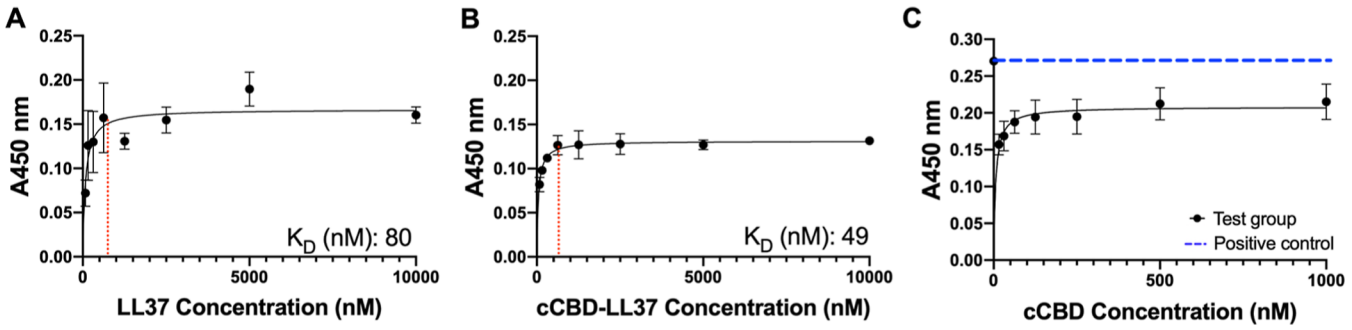

Figure 1. binding affinities of (A) LL37 and (B) cCBD-LL37 to collagen were determined. Experimental curves were fitted with saturation binding, one-site-specific binding model. (n = 4 replicates; data are mean ± S.D.). Dissociation constants [K_D] and binding capacities (red dotted line) determined from the fitted curves are shown in the figure. (C) cCBD-LL37 binding to collagen with the inhibition of cCBD. ELISA plates were coated with collagen and further incubated with cCBD and cCBD-LL37. Bound cCBD-LL37 was detected using anti-LL37 antibody. (n = 4 replicates; data are mean ± S.D.). Experimental curves were fitted with saturation binding, one-site-specific binding model.

determined by the BeStSel modeling based on CD spectral data.

2.6. Release of AMPs from Collagen Wound Dressing. PURACOL collagen type I dressing (Medline) was prepared with LL37, cCBD-LL37, or cCBD as described previously.[15] In brief, PURACOL collagen type I dressing was cut into 5 mm diameter disks using biopsy punches under sterile conditions. Scaffolds were loaded by adsorbing 5 μL of LL37 (1478 μg/mL), cCBD-LL37 (2078 μg/mL), or cCBD (610 μg/mL) in PBS, pH 7.4. Scaffolds were hydrated with the peptides or PBS control solution on hydrophobic polydimethylsiloxane (PDMS) mats, placed in a 23 °C incubator for 1 h.

After loading and incubating, the scaffolds were treated with either peptide or PBS control solutions. The scaffolds were then rinsed with pH-adjusted PBS twice, each for 5 min, and the washing buffers were collected. Next, the scaffolds were rotated on a Labquake Tube Rotator (Thermofisher) in pH-adjusted PBS release medium at room temperature. The release medium from each tube was collected at designated intervals (1 h, 4 h, 1 day, 2 days, and 4 days) and subsequently replaced with fresh medium under sterile conditions.

A direct ELISA was applied to measure peptide concentrations in the collected aliquots, as well as in the initial washing buffers. Aliquots were added into Brand microplates and incubated overnight at 4 °C. Then, the wells were blocked with 1% w/v BSA. Next, the wells were incubated with polyclonal rabbit anti-human LL37 antibody (0.4 μg/mL, AnaSpec, #AS-55927) or polyclonal rabbit anti-FLAG antibody (1 μg/mL, Millipore Sigma, #F7425). The antibody was detected by horseradish peroxidase-conjugated goat anti-rabbit antibody (0.3 μg/mL, Bio-Rad, #1706515). Color development and absorbance measurement were done as described above.

2.7. Immunohistochemistry (IHC) and Staining. After 4 days, the scaffolds were transferred into histology cassettes and fixed in 10% v/v formaldehyde. Then, the scaffolds were processed (ATP 1 tissue processor, Triangle Biomedical Sciences) and embedded in paraffin (Tissue-Tek TEC 6, Sakura). Scaffolds were cut into 5 μm sections, de-paraffinized with xylene, rehydrated in a series of 100−70% ethanol, and immersed in water for 5 min. Samples were then boiling under pressure with antigen retrieval solution followed by blocking with 5% v/v goat serum in PBS for 30 min at room temperature. Next, samples were incubated with polyclonal rabbit anti-human LL37 antibody (10 μg/mL, Anaspec, #AS55927) in 3% v/v NGS or polyclonal rabbit anti-FLAG antibody (1μg/mL, Millipore Sigma, #F7425) in 3% v/v NGS overnight at 4 °C. Then, AlexaFluor 594 goat anti-rabbit antibody (5 μg/mL, Thermo Fisher Scientific, #A11012) was added for 1 h at room temperature. After rinsing, samples were incubated with monoclonal mouse anti-collagen antibody (10 μg/mL, Thermo Fisher Scientific, #MA1-26771) in 3% v/v NGS overnight at 4 °C. Then, AlexaFluor 488 goat anti-mouse antibody (2 μg/mL, Thermo Fisher Scientific, #A11001) was added for 1 h at room temperature. The coverslip was mounted with a ProLong Gold antifade mountant (Thermo Fisher Scientific, #P36930). Images were acquired with a Keyence All-in-One fluorescence microscope BZ-800 with a 20× objective.

2.8. Statistical analysis. Statistically significant differences between experimental groups were determined by one-way ANOVA followed by Tukey's test with GraphPad Prism. For single comparisons, the Mann−Whitney U test was used.

3. RESULTS

3.1. AMPs and Collagen Binding Affinity. The binding affinity of LL37 and cCBD-LL37 to collagen was examined (Figure 1A−B). Both LL37 and cCBD-LL37 demonstrated saturable binding to collagen within the range tested, and the Scatchard plot was analyzed as a straight line (Figure S1). Based on a one-site-specific binding model, LL37 has a K_D = 80 nM and cCBD-LL37 has a K_D = 49 nM. The nanomolar (nM) range of K_D values demonstrates strong binding affinities of LL37 and cCBD-LL37 to the collagen tested. The K_D of LL37 was higher than that of cCBD-LL37, indicating more rapid dissociation; thus, LL37 bound less strongly than cCBD-LL37 to collagen.

3.2. Inhibition of AMPs Binding by Collagen-Binding Domain. We next investigated the cCBD responsible for association with collagen. ELISAs for cCBD-LL37 binding to collagen were carried out in the presence of excess cCBD. The data are shown in Figure 1A,B. Excess cCBD significantly (*p < 0.05) inhibited cCBD-LL37 binding to collagen, but cCBD-LL37 was still able to bind to collagen in a saturable behavior.

3.3. Characterization of the Interaction between Collagen and AMPs. Varying ionic strength or pH solution has been demonstrated to be a useful method for examining the presence of electrostatic interactions.[26,27] To confirm the role of the electrostatic interactions in LL37 and cCBD-LL37 binding to collagen, the binding of LL37 and cCBD-LL37

https://doi.org/10.1021/acsomega.3c05328
ACS Omega 2023, 8, 35370−35381

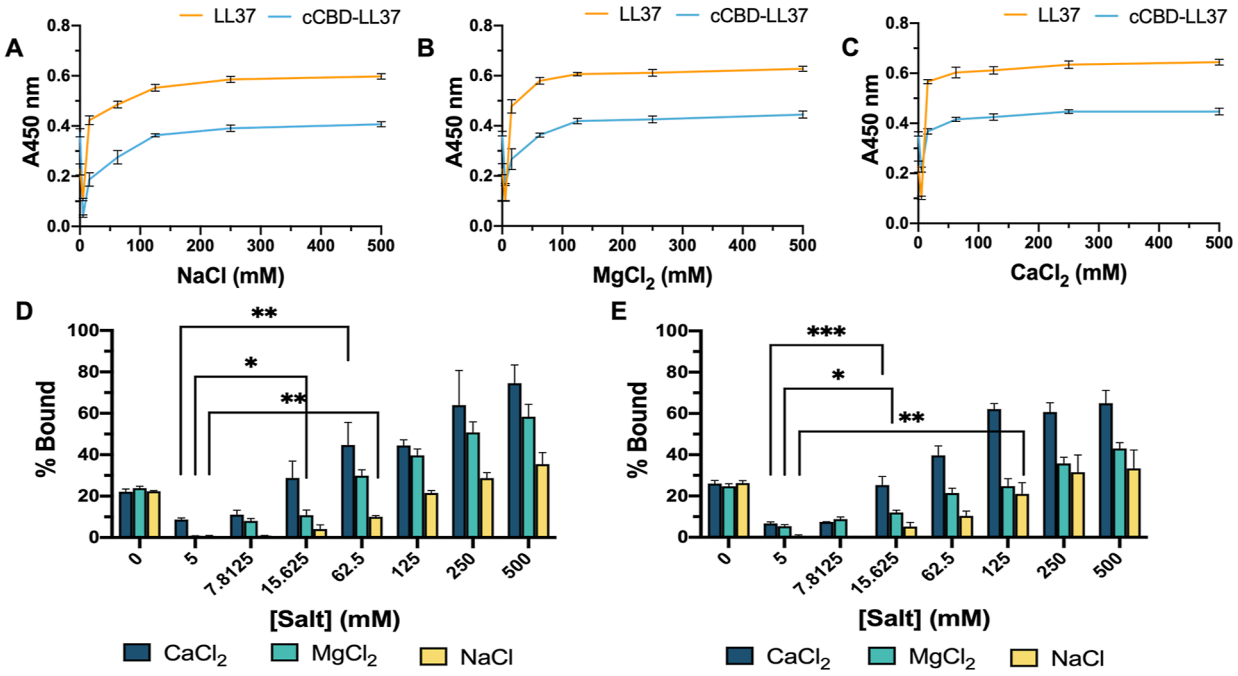

Figure 2. Effect of ionic strength on the binding of LL37 and cCBD-LL37 to collagen. Binding of 0.5 μM of LL37 and cCBD-LL37 to collagen as a function of ionic strength was measured by ELISA in various concentrations of (A) NaCl, (B) $MgCl_2$, and (C) $CaCl_2$. (n = 4 replicates; data are mean ± S.D.). (D) LL37 and (E) cCBD-LL37 binding to collagen under varying ionic strength is indicated as percentage of the initial protein loaded. One-way ANOVA Tukey's tests were performed to compare difference (n = 4 replicates; data are mean ± S.D.; *p < 0.05, **p < 0.01, ***p < 0.001).

under varying ionic strength and pH was measured. The binding of LL37 and cCBD-LL37 to collagen under varying NaCl concentration is presented in Figure 2A. Initially, the binding of LL37 and cCBD-LL37 to collagen decreased at low NaCl concentrations, but then the binding increased in a concentration-dependent manner, reaching a maximum between 150 and 250 mM NaCl. Assays containing bivalent salts, $CaCl_2$ and $MgCl_2$, were also tested and exhibited similar binding behaviors (Figure 2B,C). The bound peptides are expressed as the percentage of the initial protein loaded (Figure 2D,E). The interpreted binding values with $CaCl_2$ and $MgCl_2$ were much higher than with NaCl. The binding of LL37 and cCBD-LL37 to collagen was highest at pH 4 (Figure 3).

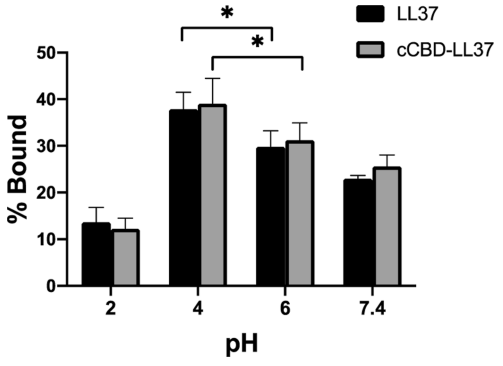

Figure 3. Effect of pH on the binding of LL37 and cCBD-LL37 to collagen. Binding of 0.5 μM of LL37 and cCBD-LL37 to collagen at pH 2.0, 4.0, 6.0, and 7.4 indicated as percentage of the initial protein loaded. One-way ANOVA Tukey's tests were performed to compare difference (n = 4 replicates; data are mean ± S.D.; *p < 0.05).

3.4. Conformation Stability of AMPs under Varying Ionic Strength and pH. CD experiments were employed to assess whether changes in the electrostatic environment induced detectable secondary structure changes in LL37 and cCBD-LL37. The first set of analyses was carried out in 5 mM phosphate buffer, pH 7.4, with varying ionic strength adjusted by NaCl. The concentration of LL37 and cCBD-LL37 was kept constant at 10 μM during all the experiments, while the NaCl concentration was increased. The CD measurements of LL37 (Figure 4A) and cCBD-LL37 (Figure 4D) all displayed two broad minima at ∼208 and ∼222 nm, indicating the existence of a helical structure. The spectra of LL37 shifted the minima slightly to the right for NaCl concentrations at 500 and 800 mM, indicating an increase in α-helical content. The spectra of cCBD-LL37 nearly overlapped at different NaCl concentrations, indicating that cCBD-LL37 had similar secondary structures at different NaCl concentrations. The content of specific secondary structures (helix, strand, turn, unordered) was determined by the BeStSel modeling based on CD spectral data as shown in Figure 4B,E.[28] Further, the helicity of LL37 (Figure 4C) and cCBD-LL37 (Figure 4F) at different NaCl concentrations was compared. The helicity of LL37 at higher NaCl concentrations (>200 mM) had a significant (***p < 0.001) helicity increase. Interestingly, no significant differences were observed for cCBD-LL37 at different NaCl concentrations.

The activity of AMPs can be inhibited in the presence of physiological serum concentrations of sodium chloride as well as divalent cations.[29,30] To investigate whether divalent cations can induce conformational changes of LL37 and cCBD-LL37, we examined the concentration-dependent effects of Mg^{2+} and Ca^{2+} on LL37 and cCBD-LL37 using 0.5, 1, 2, 5, and 10 mM $MgCl_2$ and $CaCl_2$ (normal physiological serum concentration of Mg^{2+} and Ca^{2+} are in the range of 2 ± 0.5 mM).[31] The CD

https://doi.org/10.1021/acsomega.3c05328
ACS Omega 2023, 8, 35370−35381

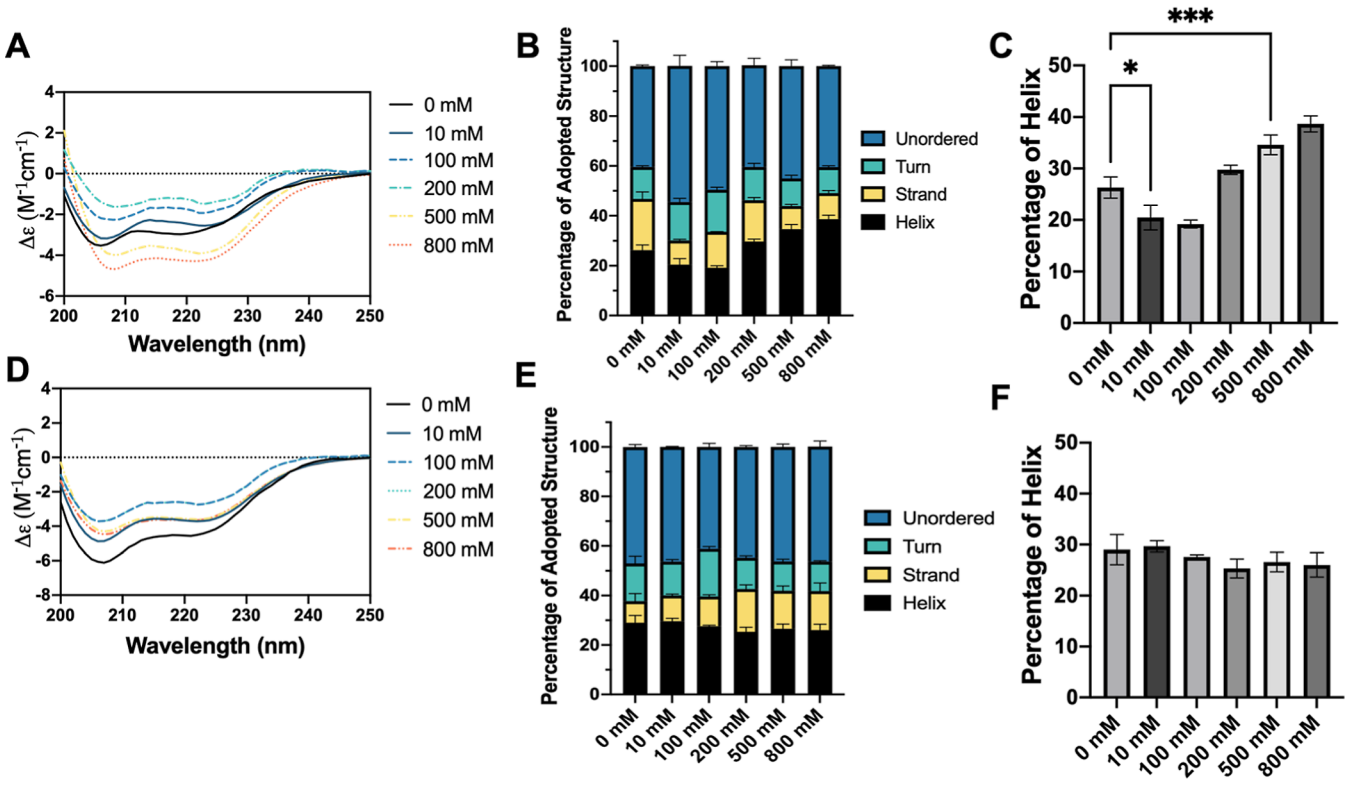

Figure 4. CD analysis of LL37 and cCBD-LL37 peptides with increasing NaCl. Representative CD spectra of 10 μM (A) LL37 and (D) cCBD-LL37 at 23 °C with increasing NaCl. From CD spectra, the content of secondary structures of (B) LL37 and (E) cCBD-LL37 in the form of helices, beta strands, turns, and unordered percentages was shown. (n = 3 replicates; data are mean ± S.D.). One-way ANOVA Tukey's tests were performed to compare difference in the percentage of the helical structure of (C) LL37 and (F) cCBD-LL37. (n = 3 replicates; data are mean ± S.D.; *p < 0.05, ***p < 0.001).

measurements of LL37 (Figure 5A) and cCBD-LL37 (Figure 5D) at different $MgCl_2$ concentrations displayed two broad minima at ∼208 and ∼222 nm. Increasing the concentration of $MgCl_2$ caused an increase in LL37 helicity (Figure 5C). The LL37 helicity at 0.5, 1, and 5 mM was significantly higher than without $MgCl_2$. For cCBD-LL37, the only α-helical percentage that was significantly altered was the helicity at 10 mM $MgCl_2$ (Figure 5D). Notably, the CD results with the bivalent salts $CaCl_2$ yielded distinct results. For LL37, in the presence of $CaCl_2$, the spectra at 0.5 and 10 mM $CaCl_2$ showed negative minima at ∼208 and ∼222 nm; the spectra at 0.5 mM $CaCl_2$ shifted the minima slightly to the right when compared with 0 mM $CaCl_2$, which indicated an increase in α-helical content, and the spectra at 10 mM $CaCl_2$ shifted the minima slightly to the left, indicating a decrease in α-helical content (Figure 6A). These two minima disappeared at 1, 2, and 5 mM $CaCl_2$ concentrations, and a positive trajectory appeared, which associated with the loss of an α-helical structure. The helicity of LL37 at 1, 2, and 5 mM $CaCl_2$ concentrations disappeared and replaced by a significant proportion of the β-strand (Figure 6B). For cCBD-LL37, the spectra minima at ∼208 and ∼222 nm were observed for the 0.5, 1, and 10 mM $CaCl_2$ concentrations, and the peaks for 1 and 10 mM were less intensive than the 0.5 mM concentration (Figure 6D). Then, the spectra trajectories of 2 and 5 mM $CaCl_2$ concentrations changed to positive with weak peaks, which indicated the loss of α-helical content. cCBD-LL37 retained α-helical content at 0.5, 1, and 10 mM $CaCl_2$ concentrations but also abolished the helicity at 2 and 5 mM $CaCl_2$ concentrations (Figure 6F).

Furthermore, to confirm the pH-dependent conformational changes of LL37 and cCBD-LL37, we examined the secondary structure of LL37 and cCBD-LL37 at pH 2, 4, 6, 7.4, and 10. Our results from CD spectra show that LL37 at pH 7.4 and 10 exhibited minima at ∼208 and ∼222 nm, indicating the presence of a helical structure (Figure 7A). However, when the pH was decreased to below 7.4, a single minimum was observed, suggesting a pH-induced relaxation toward the formation of a random coil structure (Figure 7A,B). The calculation of secondary structure shows that the helicity of LL37 is highest at pH 10 (Figure 7C). For cCBD-LL37, similarly, CD spectra show minima at ∼208 and ∼222 nm at pH 7.4, and at pH 10, similar negative features were observed at ∼208 and ∼222 nm but with greater resolution between the two peaks, indicating higher helical content. At pH 6, 4, and 2, the negative peak at ∼222 nm of CD spectra gradually diminished, indicating an unfolded or disordered conformation (Figure 7C). Similarly, the calculation of cCBD-LL37's secondary structure shows that the helicity of LL37 is also highest at pH 10 (Figure 7F).

3.5. In Vitro Release Kinetics of AMPs. The acute and chronic wound healing environment progresses from an alkaline state to a neutral and then acidic state during healing.[32,33] We hypothesized that unmodified LL37 may be nonspecifically adsorbed onto collagen and released into the surrounding media with decreasing pH, while cCBD-LL37 and cCBD with the aid of the collagen-binding domain for specific binding would have a slower and similar release profile under varying pH. To test this hypothesis, we measured peptide release from PURACOL collagen scaffolds at pH 5.5, 6, 7.4,

https://doi.org/10.1021/acsomega.3c05328
ACS Omega 2023, 8, 35370−35381

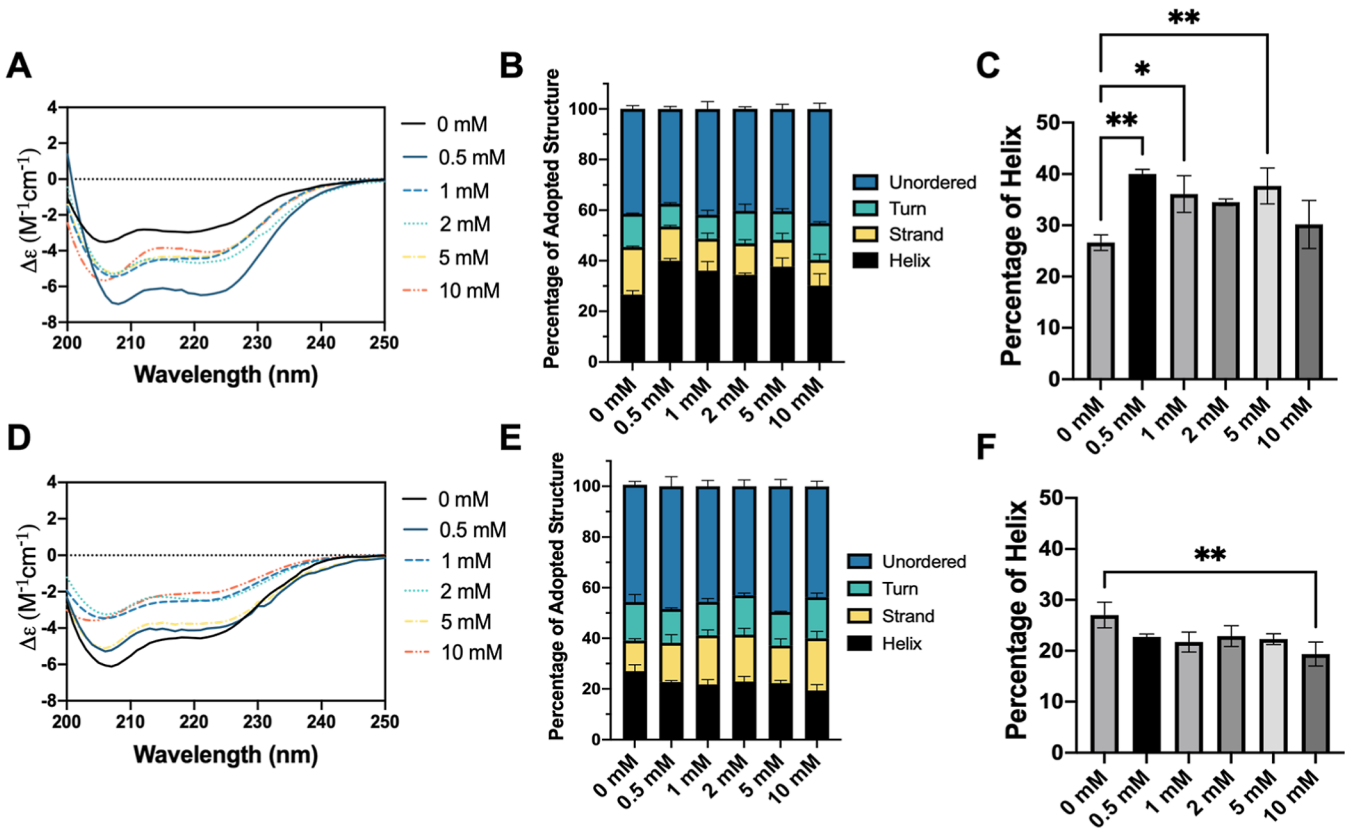

Figure 5. CD analysis of LL37 and cCBD-LL37 peptides with increasing $MgCl_2$. Representative CD spectra of 10 μM (A) LL37 and (D) cCBD-LL37 at 23 °C with increasing $MgCl_2$. From CD spectra, the content of secondary structures of (B) LL37 and (E) cCBD-LL37 in the form of helices, beta strands, turns, and unordered percentages was shown. (n = 3 replicates; data are mean ± S.D.). One-way ANOVA Tukey's tests were performed to compare difference in the percentage of the helical structure of (C) LL37 and (F) cCBD-LL37. (n = 3 replicates; data are mean ± S.D.; *p < 0.05, **p < 0.01).

and 8 by ELISA and then calculated the cumulative release profiles for each peptide (Figure 8A−C). PURACOL is composed of 100% native bovine collagen type I. It is a porous material with approximately 80% porosity of scaffold volume.[15,34]

Prior to each peptide cumulative release study, the scaffolds were rinsed twice with the release medium to remove the weakly bound peptide. The mass loss of peptide during washing procedures is expressed as a percentage of the initial protein loaded (Table 1). As shown in the table, the mass loss of LL37 increased as pH decreased, with the highest mass loss of LL37 at pH 5.5 (∼32.1%). Similarly, the mass loss of cCBD-LL37 increased as pH decreased, but the value was smaller than the mass loss of LL37; the highest mass loss of cCBD-LL37 was ∼14.6% at pH 5.5. However, the cCBD showed a higher mass loss at pH 8. The highest mass loss of cCBD was ∼16.1% at pH 8 during the washing. These results suggest that cCBD is able to enhance retention of cCBD-LL37 and cCBD on collagen scaffolds under varying pH but may also be affected by electrostatic interactions induced by varying pH.

The release profiles of LL37 showed a short burst-like release at pH 5.5 and 6, represented by an initial increase in cumulative release within the first hour (Figure 8A). The release at the first hour was ∼4.1% at pH 5.5, ∼3.6% at pH 6, with a cumulative release of ∼5.2% at pH 5.5 and ∼5.0% at pH 6 by day 4. The release at the first hour at pH 7.4 (∼0.6%) and pH 8 (∼0.5%) was much lower than at pH 5.5 and 6, and the cumulative release at pH 7.4 (∼2.0%) and pH 8 (∼1.7%) by day 4 was also lower when compared with that at pH 5.5 and 6. The cCBD-LL37 released ∼4.3% at pH 5.5 and ∼3.6% at pH 6 at the first hour, and then cCBD-LL37 release appeared comparatively sustainable through these time points with a cumulative release of ∼10.4% at pH 5.5 and ∼10.0% at pH 6 by day 4. At pH 7.4 and 8, cCBD-LL37 showed burst-like release at the first hour, reaching ∼3.1% and ∼3.4%, and ∼4.8% and ∼6.7% by day 4, respectively. The cumulative release of cCBD at all pH levels showed similar release profiles. Overall, the total mean cumulative release of cCBD after 4 days was ∼2.2% at pH 8, ∼2.0% at pH 7.4, ∼2.8% at pH 6, and ∼3.3% at pH 5.5.

The peptide-absorbed collagen scaffold samples at varying pH harvested at day 4 were immunostained to observe the retention of peptides during the release assay (Figure 9A−E). In all peptide-absorbed scaffold sample groups, peptides were observed. At pH 8, 7.4, and 6, LL37 and cCBD-LL37 showed a diffuse distribution, with enrichment around the collagen scaffolds as expected (Figure 9A−C). At pH 5.5, LL37 and cCBD-LL37 were observed along the edges of collagen scaffolds (Figure 9D). Immunohistochemistry images of cCBD-absorbed scaffolds also suggest that cCBD is retained on the scaffolds (Figure 9E).

4. DISCUSSION

The collagen-binding domain has been reported to exhibit high specific affinity for type I collagen[35−37] and enhance the retention of cCBD-LL37 on collagen.[20] However, the binding

https://doi.org/10.1021/acsomega.3c05328
ACS Omega 2023, 8, 35370−35381

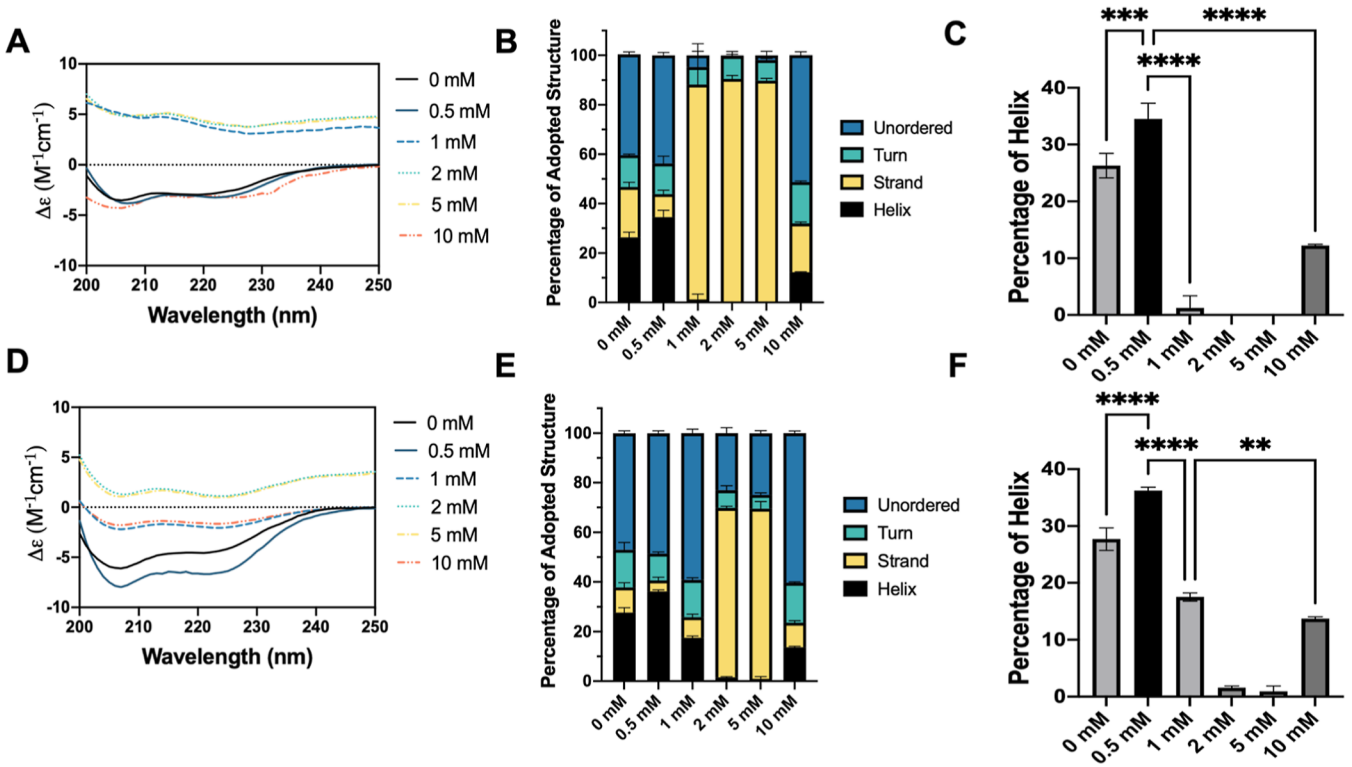

Figure 6. CD analysis of LL37 and cCBD-LL37 peptides with increasing $CaCl_2$. Representative CD spectra of 10 μM (A) LL37 and (D) cCBD-LL37 at 23 °C with increasing $CaCl_2$. From CD spectra, the content of secondary structures of (B) LL37 and (E) cCBD-LL37 in the form of helices, beta strands, turns, and unordered percentages was shown. (n = 3 replicates; data are mean ± S.D.). One-way ANOVA Tukey's tests were performed to compare difference in the percentage of the helical structure of (C) LL37 and (F) cCBD-LL37. (n = 3 replicates; data are mean ± S.D.; $^{**}p < 0.01$, $^{***}p < 0.001$, $^{****}p < 0.0001$).

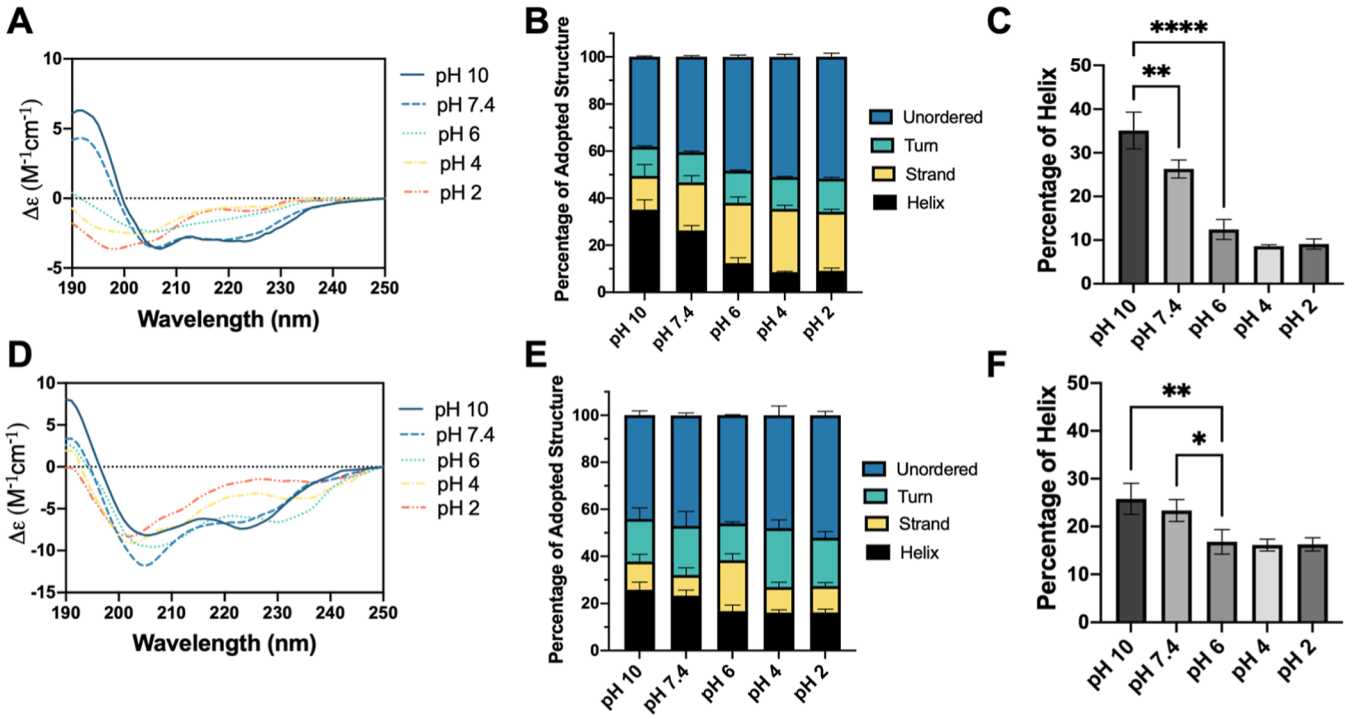

Figure 7. CD analysis of LL37 and cCBD-LL37 peptides with decreasing pH. Representative CD spectra of 10 μM (A) LL37 and (D) cCBD-LL37 at 23 °C at pH 10.0, 7.4, 6.0, 4.0, and 2.0. From CD spectra, the content of secondary structures of (B) LL37 and (E) cCBD-LL37 in the form of helices, beta strands, turns, and unordered percentages was shown. (n = 3 replicates; data are mean ± S.D.). One-way ANOVA Tukey's tests were performed to compare difference in the percentage of the helical structure of (C) LL37 and (F) cCBD-LL37. (n = 3 replicates; data are mean ± S.D.; $^{*}p < 0.05$, $^{**}p < 0.01$, $^{****}p < 0.0001$).

https://doi.org/10.1021/acsomega.3c05328
ACS Omega 2023, 8, 35370−35381

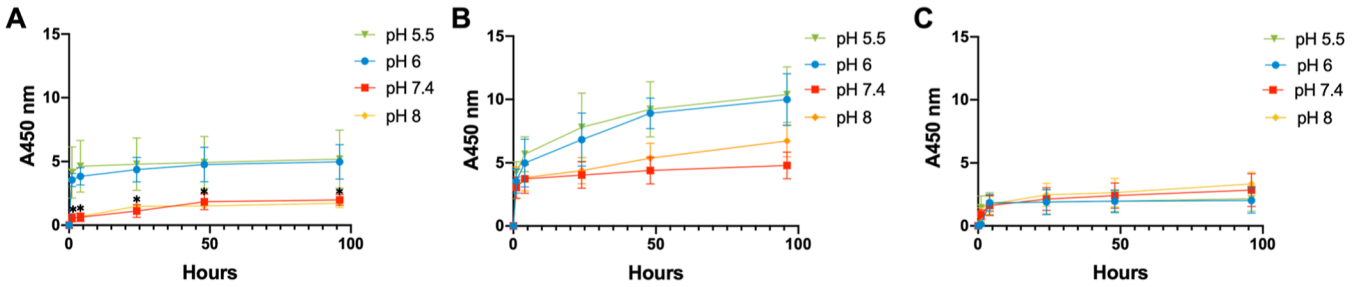

Figure 8. Cumulative release profiles for (A) LL37, (B) cCBD-LL37, and (C) cCBD from collagen scaffolds as a function of time. Statistical analyses were performed to compare cumulative release of pH 5.5, 6, and 8 with pH 7.4 at each time point. The cumulative release profiles of LL37 at pH 5.5 and pH 6 were significantly higher than LL37 at pH 7.4 and 8 at all time points. (n = 3 replicates; data are mean ± S.D.; *p < 0.05).

Table 1. Percentage Mass Loss of LL37, cCBD-LL37, cCBD during the Washing Procedures in the Cumulative Release Study[a]

mass %		LL37	cCBD-LL37	cCBD
pH 8	wash 1	1.5 ± 0.4	0.9 ± 0.1	5.1 ± 1.6
	wash 2	0.1 ± 0.08	0.8 ± 0.3	8.5 ± 0.7
pH 7.4	wash 1	11.6 ± 2.5	11.8 ± 2.9	3.3 ± 3.1
	wash 2	0.6 ± 0.09	1.22 ± 0.6	0.07 ± 0.003
pH 6	wash 1	21.3 ± 2.5	10.5 ± 0.4	1.1 ± 0.8
	wash 2	1.1 ± 0.4	2.7 ± 0.3	1.1 ± 0.1
pH 5.5	wash 1	29.4 ± 1.7	13.1 ± 1.5	1.5 ± 0.7
	wash 2	0.7 ± 0.3	1.3 ± 0.2	1.2 ± 0.06

[a]n = 3 replicates; data are mean ± S.D.

mechanism of cCBD-LL37 to collagen remains unclear. We hypothesized that the positively charged LL37 may bind nonspecifically to the negatively charged groups on the collagen surface. cCBD-LL37 possesses the same positive charge as LL37, whose nonspecific interaction is likely a contributing factor during the binding, and the cCBD may further enhance the formation of high affinity.

In this study, we first demonstrate that both LL37 and cCBD-LL37 interact with type I collagen, exhibiting comparable binding capacities (~625 nM) for collagen, and cCBD-LL37 had a slightly higher affinity for collagen than LL37 (Figure 1A,B). The theoretical binding capacities of LL37 and cCBD-LL37 were calculated as follows to compare with the experimental value (Supporting Information). The adsorbed collagen mass per well in a 96-well plate was calculated according to manufacturer's data (~0.14 μg). One-site-specific binding to collagen of collagenase binding domains to collagen triple helices was applied.[38−41] The number of collagen triple helices was determined using the molecular weight of the collagen monomer triple helix (280 kDa).[40] There are approximately 0.3×10^{12} collagenase binding sites. The moles of LL37 and cCBD-LL37 that can bind on the collagen are 4.9×10^{-13} mol and 5.1×10^{-13} mol, respectively. Therefore, the molar concentration of LL37 and cCBD-LL37 needed for saturated collagen binding is 5.4 and 5.6 nM, respectively. As the experimental binding capacity (~625 nM) is higher than the theoretical value (~4 nM), it is reasonable to assume that LL37 and cCBD-LL37 bind through one-site-specific binding to collagen. The involvement of cCBD during the binding was studied by testing the inhibition of AMPs binding by excess cCBD. The results show that the excess cCBD inhibited cCBD-LL37 binding to collagen but did not completely abrogate the binding, which implies that cCBD-LL37 binding to collagen may not be the simply one-site-specific binding through collagen-binding domain, but non-specific interactions may also be involved.

LL37 has a charge of +6 at physiological pH.[15] cCBD-LL37 retains the same +6 charge with the addition of cCBD, indicating that there is a possibility that electrostatic interactions are involved in the binding of cCBD-LL37 to collagen. The involvement of electrostatic interactions can be examined by increasing the ionic strength or decreasing the pH of the buffer used during binding.[42,43] In the present study, we examined various salt and pH changes, conditions that would be expected to disrupt charge−charge interactions between the peptides and collagen. Each of these treatments affects the binding of LL37 and cCBD-LL37 to collagen (Figures 2 and3). Electrostatic interactions have been found to be involved in protein−protein interactions in long-range electrostatic forces which lead to the formation of a low-affinity complex and then in close-range interactions which give the final high-affinity complex.[44−46] It is possible that electrostatic interactions are involved in the binding of LL37 and cCBD-LL37 to collagen, and the non-specific, long-range electrostatic interactions would develop an initial low affinity prior to the formation of close-range interactions (salt bridges). Interestingly, AMP binding to collagen was never completely abolished, even at low pH or very high salt. Furthermore, AMP-collagen binding is higher at high salt concentrations. Previous studies have shown that increased ionic strength stabilizes hydrophobic interactions.[45,47] Thus, hydrophobic interactions may also be involved in stabilization of the binding of AMPs to collagen. This explanation corresponds with the results shown in Figure 2D,E, where AMP-collagen binding was enhanced by the bivalent cations Ca^{2+} and Mg^{2+}, which may be related to their higher charge density having a greater stabilizing effect.

Several groups have reported that α-helix stability is dominant for antimicrobial activity.[48−51] An assessment of the peptide conformations in aqueous media at varying ionic strengths and pH levels can be helpful in comparing the conformational stability between LL37 and cCBD-LL37. We have shown that the helicity of LL37 (26%) and cCBD-LL37 (29%) is comparable when no salt adjustment is made (Figures 4−6). Previous studies reported a similar helical content of LL37.[52,53] The helicity of LL37 showed significant differences upon exposure to increasing salt concentrations. We observed that LL37 lost the helicity at 1, 2, and 5 mM $CaCl_2$. White et al. observed with the addition of 2.5 mM $CaCl_2$ that the minimum inhibitory concentration (MIC) of LL37 against *Escherichia coli* (ATCC 25922) and *Pseudomonas aeruginosa* (ATCC 27853) increased from 1.25 to >10 μM.[54] Turner et al. revealed that the addition of 1 mM Ca^{2+} substantially increased the MIC of LL37.[55] Moreover, the helicity decreased from 26

https://doi.org/10.1021/acsomega.3c05328
ACS Omega 2023, 8, 35370−35381

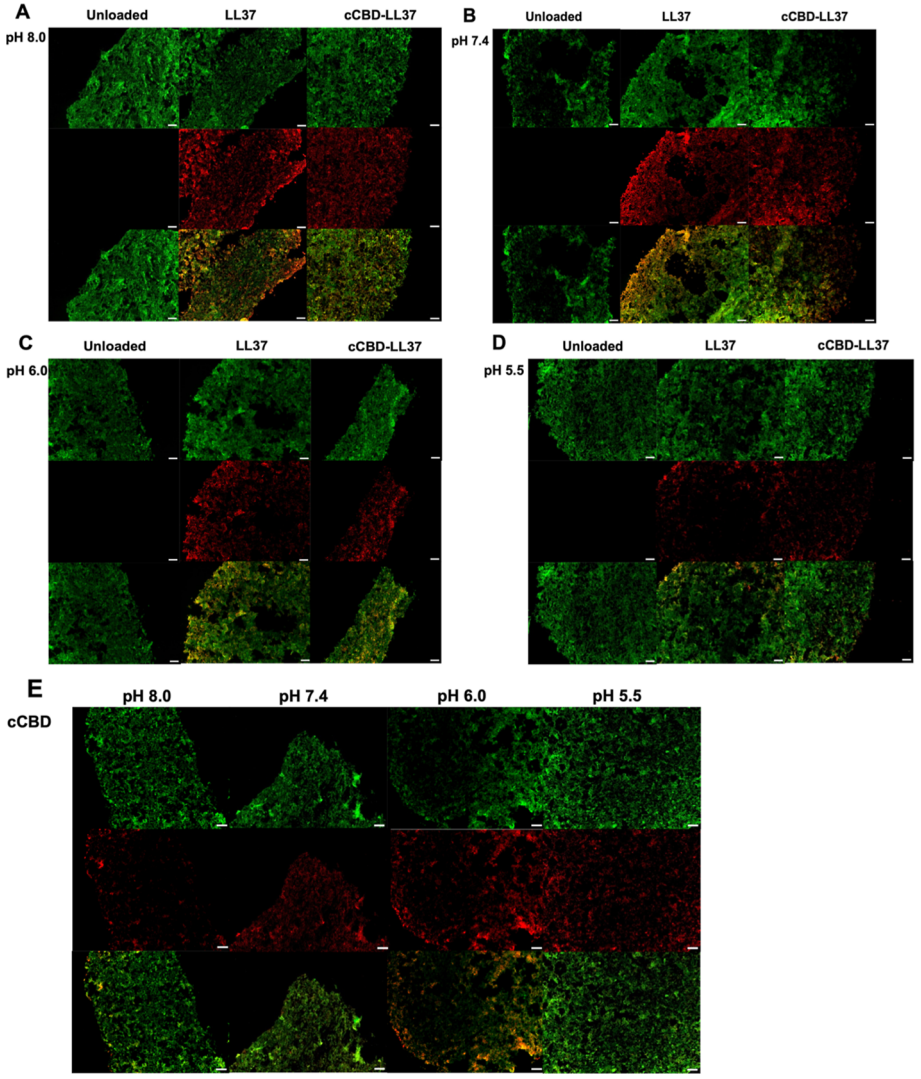

Figure 9. Representative immunohistochemistry images of scaffold sections at pH 8, 7.4, 6, and 5.5 harvested at 4 days. LL37 and cCBD-LL37 immunohistochemistry images of scaffold sections at (A) pH 8, (B) pH 7.4, (C) pH 6, (D) pH 5.5 and cCBD immunohistochemistry images of scaffold sections (E) at pH 8, 7.4, 6, and 5.5 were shown. The collagen scaffolds were identified by anti-collagen antibody (green), LL37 and cCBD-LL37 were identified by anti-LL37 antibody (red), cCBD were identified by anti-FLAG antibody (red). Scale bar = 100 μm.

to 18% with the addition of 100 mM NaCl. Turner et al. tested LL37 against Gram-positive and Gram-negative bacteria with the addition of 100 mM NaCl and showed that LL37 retained its antimicrobial activity, but the MIC increased.[55] These results are consistent with previous studies that the helical content of LL37 is correlated with antibacterial activity.[56−58] cCBD-LL37 displayed stronger structural stability at varying ionic strengths when compared with LL37, which may indicate better antimicrobial activity. Although altering the ionic strength of the buffer using different cations does cause changes in the α-helical content of the peptides, it does not seem that the specificity of the cations is responsible for the binding of peptides to the collagen, as similar binding profiles were observed.

Interestingly, both LL37 and cCBD-LL37 exhibited a decrease in helicity at low pH and an increase in helicity at high pH (Figure 7). This finding is in excellent agreement with what Johansson et al. reported for LL37 helicity changes under varying pH.[25] Johansson et al. suggested that the destabilizing interactions between positive residues can be largely affected at low pH; therefore, the conformational changes of LL37 could be due to protonation of acidic side chains, accompanied by losses of stabilizing complimentary side chain ion pairs.[25] Although LL37 and cCBD-LL37 showed similar helicity changing behavior under varying pH, cCBD-LL37 exhibited less helicity changes. Amidzadeh et al. designed a novel fusion protein that consists of KGF (keratinocyte growth factor) and cCBD, and their study revealed that the secondary structure of the recombinant peptide was better preserved when cCBD was fused to the C-terminal of KGF.[59] A possible explanation for these results is that the cCBD is a hydrophilic peptide, so this hydrophilic tail contributes to the conformational stability by forming a hydrogen bond with water.[60−62]

Our earlier findings reasoned that the electrostatic interactions are likely involved in the binding of LL37 and cCBD-LL37 to collagen. The CD results showed that the helical conformation of LL37 and cCBD-LL37 is pH-dependent. We concerned if the pH, which shifts from alkaline to neutral and then to acidic during the progression of acute and chronic wound healing, would also impact the peptide's retention on the collagen scaffolds.[32,33] We calculated the cumulative release of LL37, cCBD-LL37, and cCBD from

https://doi.org/10.1021/acsomega.3c05328
ACS Omega 2023, 8, 35370−35381

collagen scaffolds over 4 days and hypothesized that the addition of cCBD would improve the retention of LL37 on the collagen scaffold, which would lead to prolonged local bioactivities. Our data show that both cCBD-LL37 and cCBD were retained more strongly on the collagen scaffolds than LL37 during the two washing steps, suggesting that cCBD is able to enhance the retention of AMPs on collagen (Table 1). This result is consistent with our previous QCM-D assay for quantifying the AMPs binding to collagen, which suggested that there was no significant difference between LL37 and cCBD-LL37 binding with collagen, but cCBD-LL37 showed better retention on the collagen after washing with buffer.[20] The large mass loss of LL37 and cCBD-LL37 at pH 5.5 and cCBD at pH 8 during the washing step indicated that how environmental pH impacts the peptide retention. The isoelectric point (pI) of LL37, cCBD-LL37, and cCBD is 11.15, 10.53, and 6.91, respectively (ExPASy pI/MW tool). The pI of type I collagen is usually given as 4.7.[63,64] At pH 5.5 and 6, LL37, cCBD-LL37, and the collagen surface are all positively charged, so the electrostatic force between LL37 or cCBD-LL37 and collagen is repulsive. For a similar reason, cCBD and collagen are both negatively charged at pH 8 and 7.4, so the electrostatic force between cCBD and collagen is also mutual repulsion force.

When the peptides were placed in the release medium, the cumulative release profiles of cCBD-LL37 and cCBD showed no significant difference at varying pH. However, the cumulative release profiles of LL37 at pH 5.5 and pH 6 were significantly higher than those of LL37 at pH 8 and 7.4 at all time points (Figure 8). Incubation of LL37 in the release medium at pH 5.5 and 6 resulted in protonation of the amino groups in both the peptide and collagen, and the electrostatic repulsion between positively charged LL37 and collagen would accelerate drug release.[65] It is worth noting that both LL37 and cCBD-LL37 exhibited a burst-like release during the first hour, but the release profile of cCBD-LL37 appeared comparatively sustainable through these time points. This pattern of release profile has been reported to be suitable for wound infection control, since the rapid release during the first hours would kill most injury-associated pathogens, and then the slow and constant release over the following few days would keep the infection under control.[66,67]

5. CONCLUSIONS

Despite many studies reporting promising results of collagen-binding domain fusion proteins when added to a collagen-based scaffolds, the interaction between the collagen-binding domain fusion protein and the collagen-based scaffold has seldom been reported. Similarly, the effect of adding a collagen-binding domain on the conformational stability of AMPs has rarely been studied.

This study presents a comprehensive analysis of the interaction between the collagen-binding domain fusion protein (cCBD-LL37) and collagen-based scaffolds, as well as the impact of cCBD on the conformational stability of AMPs in various electrostatic environments. Our findings reveal that both LL37 and cCBD-LL37 interact with type I collagen through long-range electrostatic forces, which facilitate an initial low-affinity binding before transitioning to close-range or hydrophobic interactions. Notably, cCBD-LL37 exhibits enhanced structural stability compared to LL37 under different ionic strengths and pH conditions, suggesting potential improvements in antimicrobial activity.

Additionally, we demonstrate that cCBD could improve the retention of AMPs on collagen scaffolds, although the release of LL37 and cCBD-LL37 into the surrounding medium is influenced by the electrostatic environment. These insights contribute to the broader understanding of cCBD-AMP interactions with collagen-based scaffolds, which will be invaluable in the design and optimization of future cCBD-AMP delivery systems for biomaterial applications.

■ ASSOCIATED CONTENT

Supporting Information

The Supporting Information is available free of charge at https://pubs.acs.org/doi/10.1021/acsomega.3c05328.

Binding of LL37 and cCBD-LL37 to collagen Scatchard plot analysis; representative immunohistochemistry images of scaffold sections; and theoretical binding capacities of LL37 and cCBD-LL37 calculation (PDF)

■ AUTHOR INFORMATION

Corresponding Author

Terri A. Camesano − *Department of Chemical Engineering, Worcester Polytechnic Institute, Worcester, Massachusetts 01609, United States;* orcid.org/0000-0002-8140-7229; Email: terric@wpi.edu

Authors

Ziqi Wei − *Department of Chemical Engineering, Worcester Polytechnic Institute, Worcester, Massachusetts 01609, United States*

Marsha W. Rolle − *Department of Biomedical Engineering, Worcester Polytechnic Institute, Worcester, Massachusetts 01609, United States;* Present Address: The Roux Institute at Northeastern University, 100 Fore Street, Portland, Maine 04101, United States; orcid.org/0000-0003-2026-4700

Complete contact information is available at: https://pubs.acs.org/10.1021/acsomega.3c05328

Author Contributions

CRediT authorship contribution statement **Ziqi Wei:** investigation, formal analysis, writing—original draft. **Marsha W. Rolle:** supervision, resources, writing—review & editing. **Terri A. Camesano:** supervision, resources, writing—review & editing.

Notes

The authors declare no competing financial interest.

■ ACKNOWLEDGMENTS

We thank the National Science Foundation [IGERT Grant no. NSF DGE 1144804, STTR Grant No NSF IIP 1521294] for funding this project. We thank Andre Figueroa Milla for Keyence All-in-One fluorescence microscope BZ-800 training in the Cell Engineering Research Equipment Suite [CERES@WPI; funded by a Massachusetts Life Sciences Center 2020 Capital Award]; Claire Joswiak and WPI histology technologist Jyotsna Patel helping with tissue processing techniques.

■ REFERENCES

(1) Gonzalez, A. C. d. O.; Costa, T. F.; Andrade, Z. d. A.; Medrado, A. R. A. P. Wound healing - A literature review. *An. Bras. Dermatol.* **2016**, *91*, 614−620.

(2) Guo, S.; DiPietro, L. A. Critical review in oral biology & medicine: Factors affecting wound healing. *J. Dent. Res.* **2010**, *89*, 219−229.
(3) Farahani, M.; Shafiee, A. Wound Healing: From Passive to Smart Dressings. *Adv. Healthcare Mater.* **2021**, *10*, 1−32.
(4) Homaeigohar, S.; Boccaccini, A. R. Antibacterial biohybrid nanofibers for wound dressings. *Acta Biomater.* **2020**, *107*, 25−49.
(5) Alcock, B.; Peijs, T. *Polymer Composites−Polyolefin Fractionation−Polymeric Peptidomimetics−ollagens*; Springer, 2013; Vol. *251*. [Online]. Available:. http://www.scopus.com/inward/record.url?eid=2-s2.0-84893074415&partnerID=tZOtx3y1.
(6) Dong, C.; Lv, Y. Application of collagen scaffold in tissue engineering: Recent advances and new perspectives. *Polymers* **2016**, *8*, 42.
(7) Ramos, R.; Silva, J. P.; Rodrigues, A. C.; Costa, R.; Guardão, L.; Schmitt, F.; Soares, R.; Vilanova, M.; Domingues, L.; Gama, M. Wound healing activity of the human antimicrobial peptide LL37. *Peptides* **2011**, *32*, 1469−1476.
(8) Dürr, U. H. N.; Sudheendra, U. S.; Ramamoorthy, A. LL-37, the only human member of the cathelicidin family of antimicrobial peptides. *Biochim. Biophys. Acta Biomembr.* **2006**, *1758*, 1408−1425.
(9) Feng, X.; Sambanthamoorthy, K.; Palys, T.; Paranavitana, C. The human antimicrobial peptide LL-37 and its fragments possess both antimicrobial and antibiofilm activities against multidrug-resistant Acinetobacter baumannii. *Peptides* **2013**, *49*, 131−137.
(10) Ridyard, K. E.; Overhage, J. The potential of human peptide ll-37 as an antimicrobial and anti-biofilm agent. *Antibiotics* **2021**, *10*, 650.
(11) Mookherjee, N.; Anderson, M. A.; Haagsman, H. P.; Davidson, D. J. Antimicrobial host defence peptides: functions and clinical potential. *Nat. Rev. Drug Discov.* **2020**, *19*, 311−332.
(12) van der Does, A. M.; Bergman, P.; Agerberth, B.; Lindbom, L. Induction of the human cathelicidin LL-37 as a novel treatment against bacterial infections. *J. Leukoc. Biol.* **2012**, *92*, 735−742.
(13) Greer, A.; Zenobia, C.; Darveau, R. P. Defensins And LL-37: A Review Of Function In The Gingival Epithelium. *Periodontol* **2000**, *63*, 67−79.
(14) Wu, W. K. K.; Wong, C. C. M.; Li, Z. J.; Zhang, L.; Ren, S. X.; Cho, C. H. Cathelicidins in inflammation and tissue repair: Potential therapeutic applications for gastrointestinal disorders. *Acta Pharmacol. Sin.* **2010**, *31*, 1118−1122.
(15) Lozeau, L. D.; Grosha, J.; Kole, D.; Prifti, F.; Dominko, T.; Camesano, T. A.; Rolle, M. W. Collagen tethering of synthetic human antimicrobial peptides cathelicidin LL37 and its effects on antimicrobial activity and cytotoxicity. *Acta Biomater.* **2017**, *52*, 9−20.
(16) Lozeau, L. D.; Grosha, J.; Smith, I. M.; Stewart, E. J.; Camesano, T. A.; Rolle, M. W. Alginate Affects Bioactivity of Chimeric Collagen-Binding LL37 Antimicrobial Peptides Adsorbed to Collagen-Alginate Wound Dressings. *ACS Biomater. Sci. Eng.* **2020**, *6*, 3398−3410.
(17) Lozeau, L. D.; Youssefian, S.; Rahbar, N.; Camesano, T. A.; Rolle, M. W. Concentration-Dependent, Membrane-Selective Activity of Human LL37 Peptides Modified with Collagen Binding Domain Sequences. *Biomacromolecules* **2018**, *19*, 4513−4523.
(18) Nishi, N.; Matsushita, O.; Yuube, K.; Miyanaka, H.; Okabe, A.; Wada, F. Collagen-binding growth factors: Production and characterization of functional fusion proteins having a collagen-binding domain. *Proc. Natl. Acad. Sci. U.S.A.* **1998**, *95*, 7018−7023.
(19) Zhao, W.; Chen, B.; Li, X.; Lin, H.; Sun, W.; Zhao, Y.; Wang, B.; Zhao, Y.; Han, Q.; Dai, J. Vascularization and cellularization of collagen scaffolds incorporated with two different collagen-targeting human basic fibroblast growth factors. *J. Biomed. Mater. Res., Part A* **2007**, *82A*, 630−636.
(20) Wei, Z.; Rolle, M. W.; Camesano, T. A. LL37 and collagen-binding domain-mediated LL37 binding with type I collagen: Quantification via QCM-D. *Colloids Surf., B* **2022**, *220*, 112852.
(21) Romijn, R. A.; Westein, E.; Bouma, B.; Schiphorst, M. E.; Sixma, J. J.; Lenting, P. J.; Huizinga, E. G. Mapping the collagen-binding site in the von Willebrand factor-A3 domain. *J. Biol. Chem.* **2003**, *278*, 15035−15039.
(22) Sasaki, T.; Hohenester, E.; Göhring, W.; Timpl, R. Crystal structure and mapping by site-directed mutagenesis of the collagen-binding epitope of an activated form of BM-40/SPARC/osteonectin. *EMBO J.* **1998**, *17*, 1625−1634.
(23) Calderwood, D. A.; Tuckwell, D. S.; Eble, J.; Kühn, K.; Humphries, M. J. The Integrin α1 A-domain Is a Ligand Binding Site for Collagens and Laminin. *J. Biol. Chem.* **1997**, *272*, 12311−12317.
(24) Ishihara, J.; Ishihara, A.; Starke, R. D.; Peghaire, C. R.; Smith, K. E.; McKinnon, T. A. J.; Tabata, Y.; Sasaki, K.; White, M. J. V.; Fukunaga, K.; et al. The heparin binding domain of von Willebrand factor binds to growth factors and promotes angiogenesis in wound healing. *Blood* **2019**, *133*, 2559−2569.
(25) Johansson, J.; Gudmundsson, G. H.; Rottenberg, M. E.; Berndt, K. D.; Agerberth, B. Conformation-dependent antibacterial activity of the naturally occurring human peptide LL-37. *J. Biol. Chem.* **1998**, *273*, 3718−3724.
(26) Schreiber, G. Kinetic studies of protein-protein interactions. *Curr. Opin. Struct. Biol.* **2002**, *12*, 41−47.
(27) Zhou, H. X. Disparate ionic-strength dependencies of on and off rates in protein-protein association. *Biopolymers* **2001**, *59*, 427−433.
(28) Micsonai, A.; Bulyáki, É.; Kardos, J. BeStSel: From Secondary Structure Analysis to Protein Fold Prediction by Circular Dichroism Spectroscopy. *Methods Mol. Biol.* **2021**, *2199*, 175−189.
(29) Deslouches, B.; Islam, K.; Craigo, J. K.; Paranjape, S. M.; Montelaro, R. C.; Mietzner, T. A. Activity of the de novo engineered antimicrobial peptide WLBU2 against Pseudomonas aeruginosa in human serum and whole blood: Implications for systemic applications. *Antimicrob. Agents Chemother.* **2005**, *49*, 3208−3216.
(30) Wu, G.; Ding, J.; Li, H.; Li, L.; Zhao, R.; Shen, Z.; Fan, X.; Xi, T. Effects of cations and PH on antimicrobial activity of thanatin and s-thanatin against Escherichia coli ATCC25922 and B. subtilis ATCC 21332. *Curr. Microbiol.* **2008**, *57*, 552−557.
(31) Deslouches, B.; Islam, K.; Craigo, J. K.; Paranjape, S. M.; Montelaro, R. C.; Mietzner, T. A. Activity of the de novo engineered antimicrobial peptide WLBU2 against Pseudomonas aeruginosa in human serum and whole blood: Implications for systemic applications. *Antimicrob. Agents Chemother.* **2005**, *49*, 3208−3216.
(32) Percival, S. L.; McCarty, S.; Hunt, J. A.; Woods, E. J. The effects of pH on wound healing, biofilms, and antimicrobial efficacy. *Wound Repair Regen.* **2014**, *22*, 174−186.
(33) Gethin, G. *The Significance of Surface pH in Chronic Wounds*; Wounds UK, 2007; Vol. *3*, pp 52−56.
(34) Karr, J. C.; Taddei, A. R.; Picchietti, S.; Gambellini, G.; Fausto, A. M.; Giorgi, F. A morphological and biochemical analysis comparative study of the collagen products Biopad, Promogram, Puracol, and Colactive. *Adv. Skin Wound Care* **2011**, *24*, 208−216.
(35) Han, Q.; Sun, W.; Lin, H.; et al. Linear ordered collagen scaffolds loaded with collagen-binding brain-derived neurotrophic factor improve the recovery of spinal cord injury in rats. *Tissue Eng., Part A* **2009**, *15*, 2927−2935.
(36) Sun, W.; Sun, W.; Lin, H.; et al. Collagen membranes loaded with collagen-binding human PDGF-BB accelerate wound healing in a rabbit dermal ischemic ulcer model. *Growth Factors* **2007**, *25*, 309.
(37) Li, M.; Mondrinos, M. J.; Chen, X.; Gandhi, M. R.; Ko, F. K.; Lelkes, P. I. Co-electrospun poly(lactide-co-glycolide), gelatin, and elastin blends for tissue engineering scaffolds. *J. Biomed. Mater. Res., Part A* **2006**, *79A*, 963−973.
(38) Nordlund, T. M. *Quantittative Understanding of Biosystem: An Introsuction to Biophysics*; CRC Press, 2011.
(39) de Souza, S. J.; Brentani, R. Collagen binding site in collagenase can be determined using the concept of sense-antisense peptide interactions. *J. Biol. Chem.* **1992**, *267*, 13763−13767.
(40) Fields, G. B.; van Wart, H. E.; Birkedal-Hansen, H. Sequence specificity of human skin fibroblast collagenase. Evidence for the role of collagen structure in determining the collagenase cleavage site. *J. Biol. Chem.* **1987**, *262*, 6221−6226.

https://doi.org/10.1021/acsomega.3c05328
ACS Omega 2023, 8, 35370−35381

(41) Wu, H.; Byrne, M. H.; Stacey, A.; Goldring, M. B.; Birkhead, J. R.; Jaenisch, R.; Krane, S. M. Generation of collagenase-resistant collagen by site-directed mutagenesis of murine pro alpha 1(I) collagen gene. *Proc. Natl. Acad. Sci. U.S.A.* **1990**, *87*, 5888−5892.
(42) Xiao, L.; Honig, B. Electrostatic contributions to the stability of hyperthermophilic proteins. *J. Mol. Biol.* **1999**, *289*, 1435−1444.
(43) Tye, C. E.; Hunter, G. K.; Goldberg, H. A. Identification of the type I collagen-binding domain of bone sialoprotein and characterization of the mechanism of interaction. *J. Biol. Chem.* **2005**, *280*, 13487−13492.
(44) Honig, B.; Nicholls, A. Classical electrostatics in biology and chemistry. *Science* **1995**, *268*, 1144−1149.
(45) Mendel, C. M.; Kunitake, S. T.; Kane, J. P. Discrimination between subclasses of human high-density lipoproteins by the HDL binding sites of bovine liver. *Biochim. Biophys. Acta, Lipids Lipid Metab.* **1986**, *875*, 59−68.
(46) Kumar, S.; Nussinov, R. Close-range electrostatic interactions in proteins. *ChemBioChem* **2002**, *3*, 604−617.
(47) Ferreri, K.; Menon, K. M. J. Characterization and isolation of a high-density-lipoprotein-binding protein from bovine corpus luteum plasma membrane. *Biochem. J.* **1992**, *287*, 841−848.
(48) Lai, Z.; Tan, P.; Zhu, Y.; Shao, C.; Shan, A.; Li, L. Highly Stabilized α-Helical Coiled Coils Kill Gram-Negative Bacteria by Multicomplementary Mechanisms under Acidic Condition. *ACS Appl. Mater. Interfaces* **2019**, *11*, 22113−22128.
(49) Park, I. Y.; Cho, J. H.; Kim, K. S.; Kim, Y. B.; Kim, M. S.; Kim, S. C. Helix Stability Confers Salt Resistance upon Helical Antimicrobial Peptides. *J. Biol. Chem.* **2004**, *279*, 13896−13901.
(50) Friedrich, C.; Scott, M. G.; Karunaratne, N.; Yan, H.; Hancock, R. E. W. Salt-resistant alpha-helical cationic antimicrobial peptides. *Antimicrob. Agents Chemother.* **1999**, *43*, 1542−1548.
(51) Lee, I. H.; Cho, Y.; Lehrer, R. I. Effects of pH and salinity on the antimicrobial properties of clavanins. *Infect. Immun.* **1997**, *65*, 2898−2903.
(52) Felgentreff, K.; Beisswenger, C.; Griese, M.; Gulder, T.; Bringmann, G.; Bals, R. The antimicrobial peptide cathelicidin interacts with airway mucus. *Peptides* **2006**, *27*, 3100−3106.
(53) Al-Adwani, S.; Wallin, C.; Balhuizen, M. D.; Veldhuizen, E. J. A.; Coorens, M.; Landreh, M.; Végvári, Á.; Smith, M. E.; Qvarfordt, I.; Lindén, A.; et al. Studies on citrullinated LL-37: detection in human airways, antibacterial effects and biophysical properties. *Sci. Rep.* **2020**, *10*, 2376−2414.
(54) White, J. K.; Muhammad, T.; Alsheim, E.; Mohanty, S.; Blasi-Romero, A.; Gunasekera, S.; Strömstedt, A. A.; Ferraz, N.; Göransson, U.; Brauner, A. A stable cyclized antimicrobial peptide derived from LL-37 with host immunomodulatory effects and activity against uropathogens. *Cell. Mol. Life Sci.* **2022**, *79*, 411−417.
(55) Turner, J.; Cho, Y.; Dinh, N. N.; Waring, A. J.; Lehrer, R. I. Activities of LL-37, a cathelin-associated antimicrobial peptide of human neutrophils. *Antimicrob. Agents Chemother.* **1998**, *42*, 2206−2214.
(56) Zhang, Q. Y.; Yan, Z. B.; Meng, Y. M.; Hong, X. Y.; Shao, G.; Ma, J. J.; Cheng, X. R.; Liu, J.; Kang, J.; Fu, C. Y. Antimicrobial peptides: mechanism of action, activity and clinical potential. *Mil. Med. Res.* **2021**, *8*, 48.
(57) Zhu, X.; Zhang, L.; Wang, J.; Ma, Z.; Xu, W.; Li, J.; Shan, A. Characterization of antimicrobial activity and mechanisms of low amphipathic peptides with different α-helical propensity. *Acta Biomater.* **2015**, *18*, 155−167.
(58) Powers, J. P. S.; Hancock, R. E. W. The relationship between peptide structure and antibacterial activity. *Peptides* **2003**, *24*, 1681−1691.
(59) Amidzadeh, Z.; Rismani, E.; Shokrgozar, M. A.; Rahimi, H.; Golkar, M. In silico design of fusion keratinocyte growth factor containing collagen-binding domain for tissue engineering application. *J. Mol. Graph. Model.* **2023**, *118*, 108351.
(60) Li, M.; Mondrinos, M. J.; Chen, X.; Gandhi, M. R.; Ko, F. K.; Lelkes, P. I. Co-electrospun poly(lactide-co-glycolide), gelatin, and elastin blends for tissue engineering scaffolds. *J. Biomed. Mater. Res., Part A* **2006**, *79A*, 963−973.
(61) Osslund, T. D.; Syed, R.; Singer, E.; Hsu, E. W. J.; Nybo, R.; Harvey, T.; Arakawa, T.; Narhi, L. O.; Chirino, A.; Morris, C. F.; et al. Correlation between the 1.6 Å crystal structure and mutational analysis of keratinocyte growth factor. *Protein Sci.* **1998**, *7*, 1681−1690.
(62) Skerlavaj, B.; Gennaro, R.; Bagella, L.; Merluzzi, L.; Risso, A.; Zanetti, M. Biological characterization of two novel cathelicidin-derived peptides and identification of structural requirements for their antimicrobial and cell lytic activities. *J. Biol. Chem.* **1996**, *271*, 28375−28381.
(63) Highberger, H.; Highberger, B. J. H.. The Isoelectric Point of Collagen A Study of the Boric Acid Color Reaction of Flavone Derivatives *J. Am. Chem. Soc.* **1938**, *71*, 2302−2303.
(64) Nezu, T.; Winnik, F. M. Interaction of water-soluble collagen with poly(acrylic acid). *Biomaterials* **2000**, *21*, 415−419.
(65) Liang, P.; Zheng, J.; Dai, S.; Wang, J.; Zhang, Z.; Kang, T.; Quan, C. pH triggered re-assembly of nanosphere to nanofiber: The role of peptide conformational change for enhanced cancer therapy. *J. Controlled Release* **2017**, *260*, 22−31.
(66) Heunis, T.; Bshena, O.; Klumperman, B.; Dicks, L. Release of bacteriocins from nanofibers prepared with combinations of poly-(D,L-lactide) (PDLLA) and poly(ethylene oxide) (PEO). *Int. J. Mol. Sci.* **2011**, *12*, 2158−2173.
(67) Amariei, G.; Kokol, V.; Boltes, K.; Letón, P.; Rosal, R. Incorporation of antimicrobial peptides on electrospun nanofibres for biomedical applications. *RSC Adv.* **2018**, *8*, 28013−28023.

https://doi.org/10.1021/acsomega.3c05328
ACS Omega 2023, 8, 35370−35381